EarthArXiv cover sheet for 'Climate controls on compound solar and wind droughts in Australia'

Authors
D. Richardson[1], A. J. Pitman[1], N. N. Ridder[2]

[1] ARC Centre of Excellence for Climate Extremes, UNSW, Sydney, New South Wales 2052, Australia
[2] Suncorp Group Limited, Brisbane, Queensland 4000, Australia

Email: doug.richardson@unsw.edu.au

Peer-review statement
This manuscript is a preprint that has been submitted to *npj Climate and Atmospheric Science* and is **not** peer-reviewed.

Climate controls on compound solar and wind droughts in Australia

D. Richardson[1,*], A. J. Pitman[1], and N. N. Ridder[2]

[1]ARC Centre of Excellence for Climate Extremes, UNSW, Sydney, New South Wales 2052, Australia
[2]Suncorp Group Limited, Brisbane, Queensland 4000, Australia
[*]doug.richardson@unsw.edu.au

ABSTRACT

Solar and wind power are central to Australia's renewable energy future, which implies an energy sector vulnerable to weather and climate variability. Alignment of weather systems and the influence of large-scale climate modes of variability risks widespread reductions in solar and wind resources, and could induce grid-wide impacts. We therefore systematically analyse the relationship between compound solar and wind droughts with weather systems and large-scale climate modes of variability over multiple time scales. We find that compound solar and wind droughts occur most frequently in winter, affecting at least five significant energy producing regions simultaneously on 10% of days. The associated weather systems vary by season and by drought type, although widespread cloud cover and anticyclonic circulation patterns are common features. Indices of major climate modes are not strong predictors of grid-wide droughts, and are typically within one standard deviation of the mean during seasons with the most widespread events. However, the spatial imprints of the teleconnections display strong regional variations, with drought frequencies varying by more than ten days per season between positive and negative phases of climate modes in some regions. The spatial variability of these teleconnection patterns suggests that droughts in one region may be offset by increased resource in another. Our work highlights the opportunity for minimising the impact of energy production variability by utilising weather and climate intelligence. Exploiting the spatial variability associated with daily weather systems and the seasonal influence of climate modes could help build a more climate-resilient renewables-dominated energy system.

Introduction

Australia has committed to reducing greenhouse gas emissions to 43% below 2005 levels by 2030, and to achieve net zero emissions by 2050 [1]. A key part of this pledge is to increase the share of electricity generated by renewable sources to 82% by 2030, up from 36% in 2022. Of the 2022 share, wind power contributed almost 13%, solar photovoltaics (including rooftop) provided nearly 15%, hydropower supplied 7%, and the remainder was delivered by bioenergy [2].

An increasing reliance on renewables means the energy sector is more exposed to variations in the weather and climate [3–5]. Wind and solar power are intermittent, governed by complex sub-daily changes in pressure gradients and the movement of clouds, respectively [6–8]. Given the importance of solar and wind in transitioning to a renewable energy economy, this intermittency will need to be mitigated through technologies such as battery storage systems and dispatchable renewables like hydropower [9–12].

The Australian Energy Market Operator (AEMO) manages the National Electricity Market, which represents approximately 80% of the nation's electricity generation [1]. The AEMO grid connects five regions of eastern Australia with over 40,000 km of transmission lines and provides energy to over ten million customers. Thirty-nine Renewable Energy Zones (REZs) have been identified by AEMO as opportunities for large-scale investment in renewable energy generation and battery storage [13]. The location of the REZs, which are spread across the grid, were determined by considering factors such as resource potential and grid proximity [14].

AEMO's large jurisdiction is an opportunity for building grid resilience through the strategic placement of solar and wind farms. Although weather systems are spatially extensive (they typically have a horizontal length scale of 1,000 km or more), they bring varying conditions over eastern Australia at any one time [15–19]. Exploiting these spatial differences could minimise the variability of electricity generation across the grid by offsetting areas of low production with areas of higher production [20–25]. However, the possibility of weather-related grid-wide impacts cannot be ruled out. A combination of weather systems could align to concurrently reduce wind and solar energy potential over a large area. For example, there is a dynamical link between blocking highs that bring calm conditions over southeast Australia and cloudiness associated with tropical cyclones in Australia's north [26]. Specific to renewable energy, a weather system featuring high pressure near Australia's southwest has been related to low grid-wide supply, although not every occurrence of this weather pattern yields substantial reductions [23].

Studies for other parts of the globe have successfully linked renewable energy supply to particular weather patterns [27–29]. This can help to guarantee energy security by aiding the design of energy systems and of energy forecast tools. In contrast to these studies, the importance of relating weather patterns to grid-wide energy production in Australia has not been systematically examined. Whether, or how often, the AEMO grid is at risk from widespread, weather-induced reductions to production is not known. Large-scale climate modes of variability could also affect the likelihood of grid-wide supply issues through their role in modulating weather systems over Australia. For example, a theoretical optimal set of wind farms would still be exposed to substantial interannual variability due to the influence of El Niño-Southern Oscillation (ENSO) [25].

More broadly, the relationship between climate modes and energy-relevant processes in Australia is not well understood. In northern and eastern Australia, ENSO may account for changes in wintertime solar energy of up to 10%, with negative ENSO phases (i.e. La Niña-like conditions) associated with a reduction in solar energy [22, 30, 31]. Solar radiation also reduces during negative phases of the Indian Ocean Dipole (IOD) in winter [30]. Wind power is negatively correlated with ENSO over much of eastern and western Australia [25], implying La Niña-like conditions may enhance wind power generation in the AEMO region, but reduce solar potential. Other modes may also be useful predictors of wind and solar resource. For example, the Southern Annular Mode (SAM) characterises the meridional position of midlatitude storm track [32–34]. This suggests that the SAM could be a useful indicator of wind power variability in Australia, but has not to our knowledge been explicitly examined.

The relative lack of research on this topic is surprising given such efforts have proved fruitful for other regions globally [10, 35, 36]. Furthermore, concurrent climate anomalies over large spatial scales (like the AEMO grid) are known to be modulated by climate modes [37–43]. A systematic analysis of the impact that climate modes have on Australia's wind and solar resources could be of great value in planning farm locations and for seasonal forecasting of renewable resources.

We assess the spatial and temporal variability of days featuring low solar and wind energy potential, which we call 'droughts'. We limit our assessment to the resource potential, focusing on the physical climate variables i.e. wind speed and solar radiation. Previous studies have estimated wind and solar power generation using empirical relationships [4, 28]. However, this approach adds a layer of uncertainty due to the many complex factors governing renewable energy production, such as plant capacities and operational procedures. Since a major component of our analysis is to identify weather patterns and climate modes associated with energy droughts, we prefer to model their relationship with physical climate variables directly.

We target our analysis on the National Electricity Market, which represents approximately 80% of the nation's electricity generation [1], and we focus on the potential for large scale, grid-wide impacts. This is achieved by analysing the individual and simultaneous (compound) occurrence of solar and wind droughts across multiple REZs at the same time. We then identify the synoptic processes associated with these events for each drought type. Finally, we examine the role of major climate modes of variability in modulating the seasonal frequency of droughts, and discuss the potential for using these climate modes in risk assessments. To the best of our knowledge, this is the first study to systematically analyse the relationship between compound solar and wind droughts with large scale weather and climate patterns over a range of time scales.

Results

Solar, wind and compound droughts

Of the 39 REZs, we consider the 36 that have existing or planned capacity for solar or wind power (the remainder are hydropower only). Seven REZs are solar only, ten are wind only, and the remaining 19 feature both (Fig. 1a). Using the ERA5 reanalysis product [44], we define a solar or wind drought as when the daily mean solar radiation or wind speed, respectively, falls below the 25th percentile of the 1959 – 2021 climatology, which is computed over all REZs. The reason we choose a relatively moderate drought threshold is primarily because we also examine compound solar and wind droughts, which we define as when a solar drought and a wind drought occur on the same day in the same location (see 'Methods'). An extreme impact can arise as a result of the co-occurrence of multiple events that are not themselves extreme, something that has been shown in a European energy context [28, 45].

There are regional differences in how often solar, wind and compound droughts occur. The seasonal cycle dominates the spatial variability of solar droughts, with REZs north of 35°S affected by fewer droughts than the REZ-wide average, and vice versa for southern regions (Fig. 1b). The frequency of wind droughts exhibits a more complex geographical pattern. Western regions, particularly in South Australia and Victoria, are less susceptible to wind droughts than eastern regions (Fig. 1c). This is due to their exposure to the mid-latitude storm track, which guides regular weather fronts over southern Australia [46]. The intensity of these fronts can dissipate as they move across land towards eastern regions. We note that the two offshore wind REZs near Sydney stand in contrast to land-based REZs in the East. The comparatively lower risk of wind droughts is due to the greater availability and consistency in offshore wind resource compared to onshore [47]. The geographic variability of compound droughts is dominated by that of solar droughts (Fig. 1c). As many of the wind- or solar-only REZs are situated in the South, only four REZs (three in Tasmania, one in Victoria) display a higher-than-average risk of experiencing compound droughts.

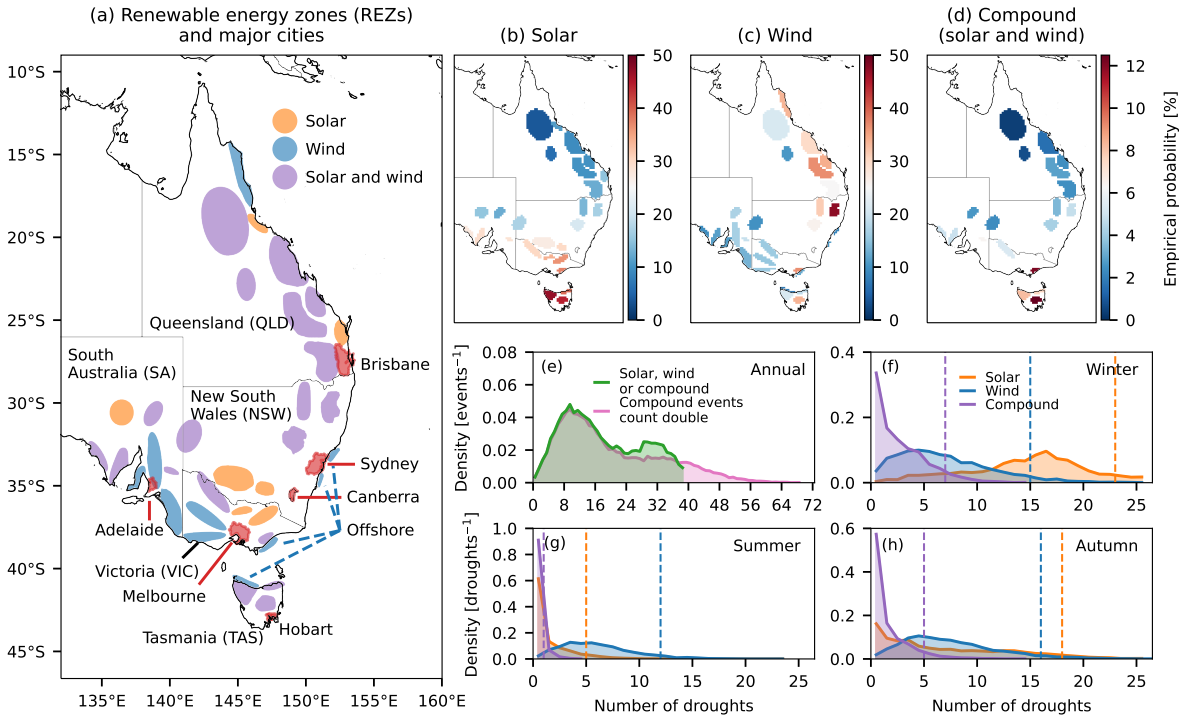

Figure 1. Study region and drought likelihoods. a Renewable Energy Zones (REZs) coloured according to the energy type they produce: solar (seven REZs), wind (10) or both (19). Major cities are shown in red. **b-d** Empirical probability (percentage of days) of a solar, wind or compound (solar and wind) drought occurring on any day in the year. Only REZs that produce the relevant energy type are shown. White shading indicates that a solar or wind drought occurs at the same frequency as the all-REZ average (25%). In **d**, white shading indicates that compound droughts occur at the frequency expected by chance if wind and solar were independent ($0.25^2 = 6.25\%$). **e** Probability density function (PDF) of the number of REZs that are simultaneously affected by any drought, with compound droughts counted as single (green) or double (pink). **f-h** PDFs of the number of REZs that are simultaneously affected by either a solar, a wind or a compound drought during winter, summer or autumn. Results for spring are omitted as they are similar to those for summer. Vertical dashed lines indicate the 95th percentile of the number of REZs in drought per day, which is the threshold used to define widespread droughts.

All three types of drought regularly occur in multiple REZs at the same time. On half of all days, 15 or more REZs simultaneously experience a drought of some kind (green line in Fig. 1e). On roughly one in five days, 28 or more REZs will experience simultaneous droughts. Compound droughts can have a greater impact on renewable energy generation than univariate (individual) droughts, as reductions in energy supply from one energy type cannot be compensated for by another. If we assume that compound droughts have twice the impact of univariate droughts, and count them as double, 10% of days have historically featured more than 39 droughts across the REZs (pink line). This highlights the vulnerability of the grid to weather patterns that have widespread implications for wind and solar resources.

We find that compound droughts in winter can be more widespread than in other seasons, especially compared to summer (purple lines in Fig. f-h). It is not particularly unusual for over five REZs to simultaneously experience a compound drought (10% of winter days; Fig. 1f). In contrast, no more than one REZ is affected by a compound drought during 95% of summer days (Fig. 1g). This is again a result of the seasonal cycle, with widespread solar droughts common in winter and rare in summer (orange lines). The spatial extent of wind droughts is relatively stable throughout the year (blue lines). The main difference is a lower likelihood of more than ten simultaneous wind droughts in spring and summer compared to winter and autumn.

Synoptic weather during widespread droughts

We next examine the synoptic weather conditions associated with widespread solar, wind and compound droughts in each season. By 'widespread', we mean the 5% of days that feature the greatest number of REZs simultaneously in drought, shown by the vertical dashed lines in Fig. 1f-h ('Methods').

Unsurprisingly, widespread solar droughts in all seasons are characterised by anomalously cloudy conditions across eastern

Australia (Fig. 2, left column), with many areas up to 55% cloudier than usual. This appears to be driven by moist, on-shore easterly flow, guided by an anticyclone in the Tasman sea. In winter, only one REZ, in far North Queensland, does not regularly feature in widespread solar droughts (Fig. 2a). In summer, there is a greater variety of REZs that comprise these events (Fig. 2g). Since the southern REZs are exposed to long daylight hours, widespread summer solar droughts most commonly feature the northern Queensland REZs. In this tropical region, summer is the wet season (and so has greater cloud cover) and, being closer to the equator, features fewer daylight hours relative to higher latitudes.

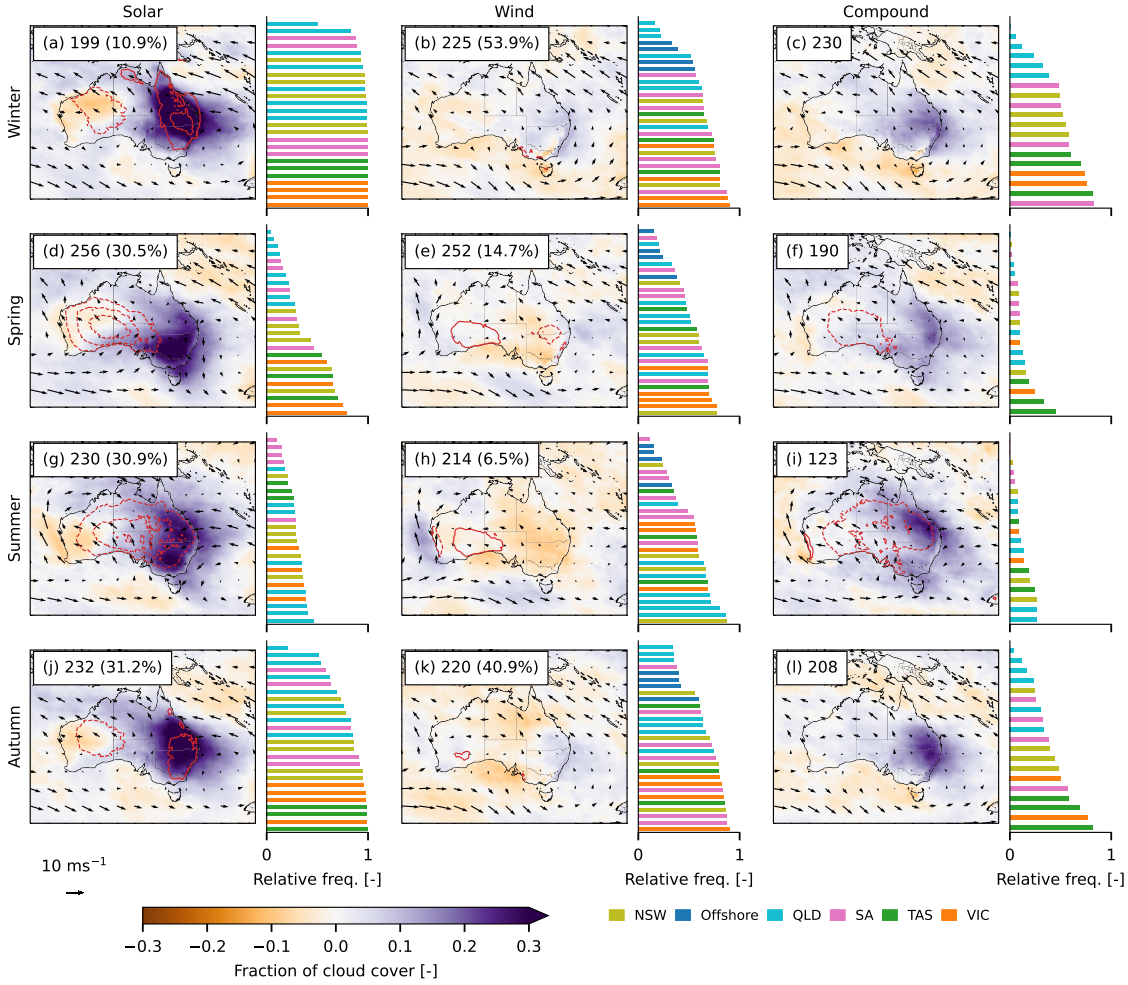

Figure 2. Synoptic weather during widespread droughts. Daily composites of the 5% most widespread drought days by season. The maps show fraction of cloud cover anomalies (shading), wind speed and direction (ms^{-1}; arrows), and daily mean 2 m temperature anomalies (red contours, starting at ± 1°C and spaced in intervals of 1°C). Solid contours are for positive values, dashed contours for negative values. The sample size of each composite is shown in the top left. For wind and solar droughts, the percentage of days shared with the compound drought composite is shown in parentheses. Bar plots to the right show the relative frequency that each REZ participates in the widespread droughts that make up each composite, coloured by state.

Widespread wind droughts feature anticyclonic conditions over eastern Australia during winter, spring and autumn (Fig. 2, middle column). In general, the anticyclone is located over Victoria and New South Wales, with the REZs in these states, plus South Australia, being the most affected during widespread drought days. The anticyclonic conditions at the surface are supported by anomalously high geopotential heights in the mid-troposphere just south of Tasmania (Fig. S1 in the supplementary information). In summer, as with solar droughts, it is the northern REZs that feature most commonly in widespread wind droughts (Fig. 2h). The 100 m wind pattern resembles those of the other seasons, but the tropospheric circulation anomalies differ substantially (Fig. S1). There is no anticyclonic anomaly near Tasmania, rather a trough extends towards southwest Australia. This may help to direct weather systems over South Australia rather than regions further east, explaining the state's

REZs' relatively infrequent role in summer wind droughts.

The 100 m winds during compound droughts in winter and autumn look remarkably similar to those during wind droughts (Fig. 2c, l versus Fig. 2b, k). The obvious difference between the two drought types (comparing middle and right columns) is in the cloudiness of compound droughts compared to wind droughts. The similarity of the wind and compound drought composites is particularly notable given they only share 54% and 41% of days for winter and autumn, respectively. In contrast, the weather pattern associated with compound droughts in spring differs from that of wind droughts (Fig. 2f). Here, still conditions are present across southern Australia. This is potentially due to a southerly displacement of the jet stream as evidenced by anomalously high geopotential heights south of the continent (Fig. S1). In summer, widespread compound droughts are infrequent, with only 123 days comprising the top 5% of summers in terms of the number of simultaneous droughts across REZs (Fig. 2i). The weather pattern exhibits very similar characteristics to widespread solar droughts in the same season (Fig. 2g), and these events show the same prevalence of northerly REZs. Furthermore, the atmospheric circulation is similar at the surface and at higher altitudes (Fig. S1). Twin anomalous highs are present over southwest Australia and east of New Zealand, resulting in light southerly and easterly flow across eastern Australia.

The regions containing REZs also exhibit anomalies in 2 m temperature during solar droughts (Fig. 2a, left column) and during compound droughts in summer (Fig. 2i). This could imply changes to energy demand through household heating or cooling requirements. We find that the temperatures in winter are warmer than normal due to the insulating effects of increased cloud cover (Fig. 2a). In summer we observe the opposite effect, with cloud cover reducing insolation and therefore temperatures (Fig. 2g). In both cases, the presumed effect of these temperature anomalies would be to reduce heating and cooling demand, not exacerbate it.

Large-scale climate associated with droughts

We now assess the role of three major climate modes of interannual variability – the El Niño-Southern Oscillation (ENSO), the Indian Ocean Dipole (IOD) and the Southern Annular Mode (SAM) – in modulating solar, wind and compound drought occurrences. We average sea-surface temperature (SST) and mean sea-level pressure (MSLP) anomalies over the seven seasons during which the mean number of simultaneous droughts is in the top 10% ('Methods').

We find that widespread solar droughts are accompanied by large scale climate anomalies that implicate ENSO and the SAM in some seasons (Fig. 3, left column). In spring and summer, there is a clear La Niña-like signature (Fig. 3d, g). This accords with our understanding of the relationship between ENSO and Australian climate, with La Niña typically associated with cooler, wetter conditions in eastern regions [48, 49]. In autumn, eastern-Pacific El Niño events may be associated with widespread solar droughts, but the magnitudes of the SST anomalies are weak (Fig. 3j). In winter, the SAM could be a key modulator of widespread solar droughts. We find substantial negative MSLP anomalies over Antarctica that resemble a positive phase of the SAM (Fig. 3a). This implies a poleward shift of the storm track away from Australia which can result in increased onshore easterly flow and greater rainfall in the east [48]. Although there is no evidence of the role of ENSO in this case, positive phase SAM events during summer can occur more frequently during La Niña events [50, 51].

Widespread wind droughts are associated with El Niño-like SST anomalies in all seasons except winter, during which ENSO is in its neutral phase (Fig. 3, middle column). The main feature during winter is a node of positive MSLP anomalies, up to 300 Pa above average, to the southeast of Australia (Fig. 3b). In spring, a band of anomalously high pressure reaches across southern Australia (Fig. 3e). In both seasons, these MSLP anomalies may reflect an increase in anticyclonic activity or a southerly shift of the storm track. These composites do not implicate the SAM, however, as they do not show negative MSLP anomalies over Antarctica, in contrast to what we found for solar droughts (Fig. 3a).

Finally, we find that widespread compound droughts are linked to ENSO and the SAM (Fig. 3, right column). These droughts are associated with a La Niña signature, although the SST anomalies are not as large in magnitude as for solar droughts during summer. The signature is, however, present in all seasons except autumn, with the strongest expression in spring. Negative MSLP anomalies over Antarctica further suggest the role of the SAM, again in all seasons except autumn. These seasons additionally feature positive MSLP anomalies south of New Zealand, which is a feature of wind droughts but not solar droughts. This implies that while the large-scale climate associated with compound droughts is most broadly similar to that of solar droughts (La Niña-like SSTs and positive SAM MSLP patterns), there are commonalities in the surface circulation between wind and compound droughts that help to explain the co-occurrence of cloud cover and weak winds.

Climate mode influence on drought frequencies

The composite results implicate ENSO and the SAM in modulating the seasonal frequency of widespread drought occurrences. However, this may be misleading. In context of the seasonal climatology, the values of climate mode indices during the seven most widespread drought seasons do not indicate a preferred phase. For example, the Niño3.4 index value is within ± 1 standard deviation of the mean during five of the seven most widespread compound droughts in winter (Fig. 4a). Although the index does skew negative for these seven winters, the result shows that not all widespread compound droughts are associated with La Niña. However, there seems to be very little chance of these droughts occurring during El Niño conditions.

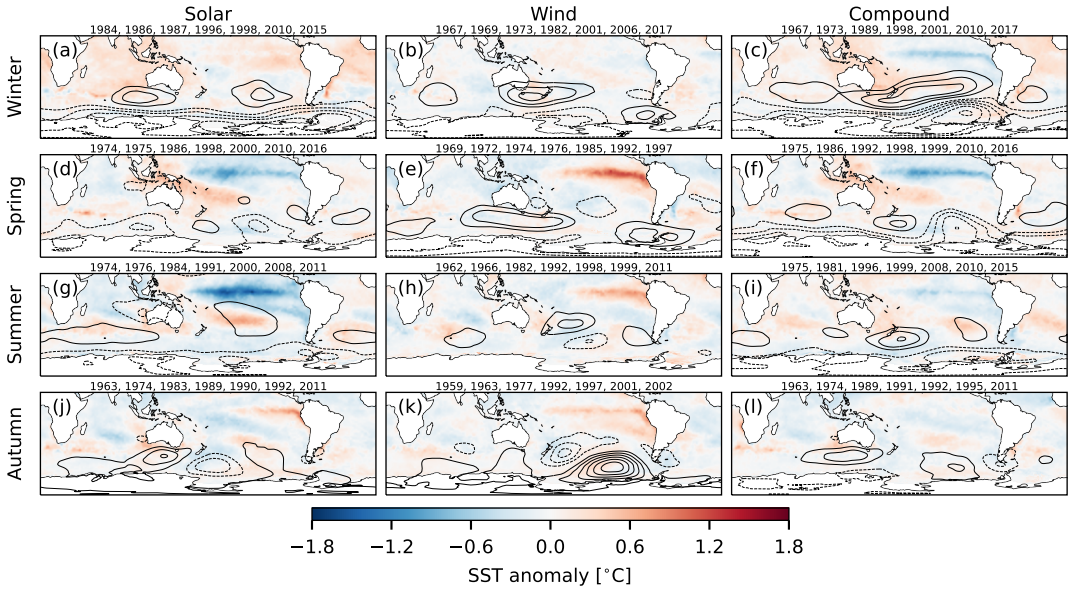

Figure 3. Large-scale seasonal diagnostics. Seasonal anomalies of sea-surface temperature (SST, measured in °C; shading) and mean sea-level pressure (contours, starting at ±100 Pa and spaced in intervals of 100 Pa, with dashed contours for negative values) composited on seasons during which the seasonal mean number of droughts per day is in the top 10% (seven seasons). The years that these seasons occurred in are displayed above each panel.

The SAM's association with widespread droughts is also unclear. We find that only two of the seven widespread solar drought winters featured strongly positive values of the SAM index (Fig. 4c). For the other five winters, the SAM is neutral, suggesting that the strong MSLP anomalies in the composite (Fig. 3c) are dominated by two winters. During widespread compound droughts, there is a clear positive skew in the values of the SAM index (Fig. 4c), but these index values are within one standard deviation of the mean in three of the seven winters. The deeply negative MSLP anomalies over Antarctica shown in the composite are substantially skewed by the winters of 1998 and 2010, during which the SAM index was 3.4 in both years. We note, however, that widespread compound droughts are unlikely to occur during a negative phase of the SAM.

We draw similar conclusions from our results for other permutations of climate modes, droughts and seasons. The strong La Niña-like SST anomalies for solar and compound droughts in spring and summer are not matched by consistent negative Niño3.4 values (figures S2 and S3). While the index values do skew negative, three or four winters lie within one standard deviation of the mean. The clearest result in favour of ENSO's role is for solar droughts in summer, with five of the seven Niño3.4 values being less than -1.5°C.

It is possible that our focus on particularly widespread droughts hides some of the influence imparted by climate modes, which exhibit spatially variable teleconnections to surface climate [48]. To investigate this, we examine drought frequencies for individual grid cells and compare results between positive and negative phases of each mode. We also consider Australia as a whole, rather than only REZs, as this could provide insight into which regions other than REZs might be considered for renewable energy planning.

Each climate mode has a relatively spatially consistent relationship with solar drought occurrences across eastern Australia (Fig. 4d-f). La Niña, negative IOD and positive SAM phases are associated with increased solar drought frequencies over large areas, in some places in excess of ten days per winter. The greatest effect is seen in New South Wales and southern Queensland. In other parts of east Australia, such as Tasmania and far north Queensland, the signal can be close to zero.

The spatial imprint of these modes' teleconnection to wind and compound droughts is more variable (Fig. 4g-l). They are in general characterised by higher drought frequencies associated with positive phases of each mode in southern Australia (except Tasmania) and along the southeastern coastline. Farther north, we find negative phases of the modes are associated with more droughts, except in far northern Queensland during positive ENSO. Wind drought frequencies can differ by over ten days per season between opposing phases of the climate modes. The differences in compound drought frequency are smaller. This is expected given their relative rarity (Fig. 1f), but they can still exceed ten days per season in some parts of southeast Australia (Fig. k-l).

In other seasons, the teleconnection patterns are broadly similar (figures S2, S3 and S4). We briefly discuss the main

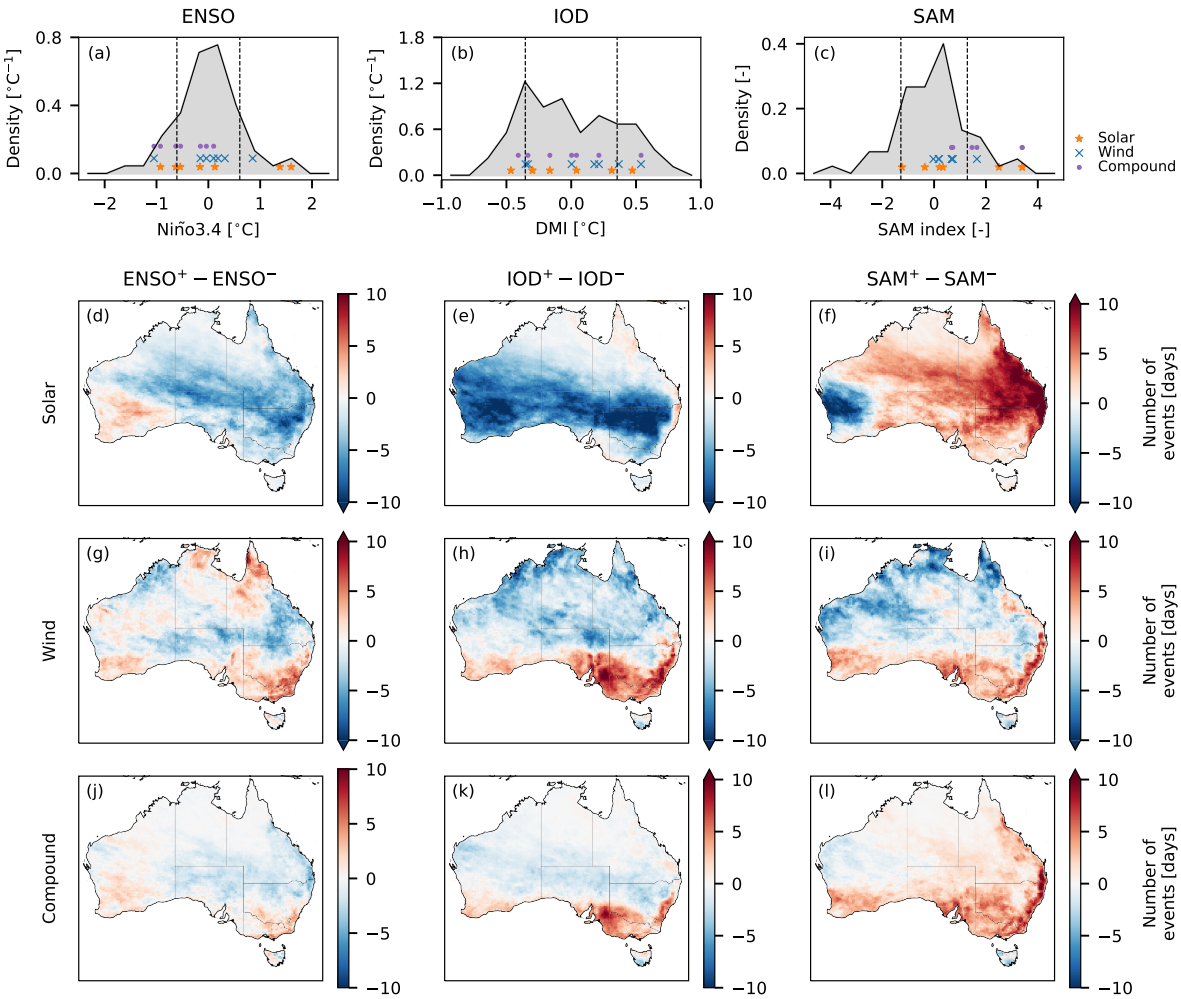

Figure 4. Climate mode influence during winter. a-c Probability density functions of winter-averaged ENSO (measured by Niño3.4), the IOD (DMI) and SAM (SAM index). Dashed lines indicated one standard deviation above or below the mean (zero). Markers indicate the mode index value during the seven winters of spatially-extensive droughts shown in Fig. 3**a-c**. **d-j** Difference in the number of winter drought days between positive and negative phases of each climate mode. A positive phase is when the index value exceeds one standard deviation above the mean, and vice versa for a negative phase.

differences here. The biggest contrast is that the magnitude of the difference between solar and compound drought frequencies during positive and negative mode phases is smaller than in winter. This is due to the overall lower solar drought frequency, and hence compound drought frequency, outside of winter. The magnitude of the difference for solar drought frequencies is generally less than |10| days per season. For compound droughts the difference is typically less than |5| days per season. In summer, the relationship between solar droughts and the IOD is the opposite to during winter, with a positive IOD phase associated with more droughts, particularly in the far northeast (Fig. S3). In summer and autumn, the relationship between the climate modes and wind droughts is more spatially variable. The eastern seaboard exhibits a negative relationship between drought frequency and positive-phase IOD and SAM (figures S3 and S4).

Discussion

Our motivation for this work was to assess the risk posed by widespread solar, wind, and compound (solar plus wind) droughts to Australia's largest electricity market, managed by the Australian Energy Market Operator (AEMO). We approached this by focusing on the synoptic weather patterns and large-scale climate modes of variability that are associated with widespread droughts across 36 Renewable Energy Zones (REZs). We believe this is the first study that systematically assesses the role of weather systems and climate modes as controls on the frequencies of compound solar and wind droughts.

We found that solar, wind and compound droughts can occur simultaneously across multiple REZs on any given day. This is in part due to our choice of moderate solar and wind drought thresholds (25% of the all-region climatology). Our results showed that there are days with particularly widespread droughts. The seasonal cycle has a strong bearing on how widespread solar droughts can be, while the extent of wind droughts changes comparatively little throughout the year. The net result of this is a higher exposure to widespread compound droughts in winter due to reduced insolation, although any drought type can occur in any season.

Our analysis showed that the weather patterns associated with widespread solar droughts are different to those associated with wind droughts. This accords with the simple assumption that a still day is more likely to be sunny and a windy day to be cloudy. Compound droughts do occur, however, and we found that in winter and autumn the weather systems during these events resemble those during wind droughts. The significant point of difference is that compound droughts feature much more cloud cover. The physical mechanism that explains very similar circulation patterns bringing different levels of cloud cover is not clear from our chosen diagnostics, but could relate to ocean temperatures and associated moisture transport [52, 53].

Widespread solar and compound drought days are associated with surface temperature anomalies. Promisingly, the sign of these anomalies implies a reduction in energy demand from heating or cooling requirements. This suggests that widespread droughts do not typically coincide with days of high demand, reducing their potential impact on the network. However, we only considered changes in daily mean temperature, and ignored factors such as population density. It would be valuable in future work to incorporate more tailored demand metrics, such as heating and cooling degree days in major cities, and analyse the relationship between these and energy production droughts.

Finally, we highlighted the resilience of the AEMO grid to three major climate modes of variability – El Niño-Southern Oscillation (ENSO), the Indian Ocean Dipole (IOD) and the Southern Annular Mode (SAM). During seasons featuring many widespread drought events, the climate modes often had no preferential phase, and the index values were often within one standard deviation of the mean. This is due to the spatial variability of the climate mode teleconnections. The AEMO grid spans a large area, with intra-grid regions often opposing in the sign of the teleconnection. The most widespread droughts therefore may not be predictable based on the phase of major climate modes. Regional droughts however, such as in individual states, may benefit from knowing the current or predicted state of climate modes.

The geographic variability of these teleconnections is an advantage for the grid. Our work implies that the occurrence of ENSO, IOD or SAM events would likely not have implications for the production of solar or wind energy across the entire grid. While one or more states may be simultaneously impacted by reduced generation potential, it is likely that other areas will not be impacted and may even experience an increase in generation potential. This highlights the opportunity for minimising production variability by ensuring adequate provision of facilities in areas that have opposing relationships to climate modes [25]. Our results also imply that meeting energy demand with solar and wind power would benefit from a hypothetical connection of the AEMO grid with southwest Australia [25]. An east-west split in the teleconnection of climate modes on solar production could provide an opportunity for transmitting power from regions of low to high shortfall.

Ultimately, better understanding the weather and climate processes that govern the variability of renewable energy resources can help to prioritise the development of certain REZs, and to manage supply and demand, and hence electricity prices [28, 54, 55]. Knowledge of the weather patterns associated with renewable energy droughts can be a useful tool in subseasonal and seasonal prediction. Climate models are more reliable in their representation of large-scale features such as climate modes than for small-scale variables [56]. This can be exploited by 'bridging' between model forecasts of climate modes and renewable energy-relevant variables, helping the energy sector manage season-to-season resource planning. Successful examples of bridging are plentiful in the literature [57–62], and seasonal forecasts of climate modes are routinely used to help decision-makers assess the possible risks to their sector [63]. We have provided here a foundation that can help to inform renewable energy planning and resource management in Australia.

Methods

Renewable Energy Zones

Renewable Energy Zones (REZs) are regions that have been identified by the Australian Electricity Market Operator (AEMO) as having high potential for the development of renewable energy generation [14]. The location of the REZs was determined according to estimated wind and solar resource potential plus social and technical constraints including the proximity to the electrical network, existing infrastructure such as roads, and population density [13].

Solar, wind and compound droughts

We use climate variables derived from the ECMWF ERA5 reanalysis product as proxies for renewable energy resource, with wind speed and solar irradiance representing wind and solar power, respectively. Both variables are computed as daily means from the hourly ERA5 reanalysis product at a spatial resolution of 0.25° [64]. For the period 1959 through 2021, we compute

100-metre wind speeds (ms^{-1}) as $w_{100} = \sqrt{u_{100}^2 + v_{100}^2}$, where u_{100} and v_{100} are zonal and meridional 100 m wind components, respectively. This level is commonly used to represent the range of typical turbine hub heights [25, 29]. We estimate solar energy potential using the mean surface downward short-wave radiation flux (Wm^{-2}). Given the importance of the diurnal cycle to energy, we define a day as 24 hours from 1400 UTC, which is equivalent to midnight local time for most of our study region. For part of our analysis we compute the average of these variables over grid cells within each REZ, with cells assigned to a REZ if their centre lies within the REZ perimeter.

We define a solar or wind drought as when the relevant climate variable falls below the 25th percentile of its climatology on a given day. These thresholds are computed over the entire time period (1959 – 2021) and over all REZs. The threshold for wind drought is 4.2 ms^{-1}, and 133 Wm^{-2} for solar drought. We do not account for zero production arising from wind speed exceeding cut-off thresholds (when turbines are shut down to prevent damage). Defining these thresholds using all REZs means that drought frequencies can be compared regionally, rather than each REZ being equally susceptible to droughts that are of different magnitudes. It also reflects the fact that wind turbines and photovoltaic panels have fixed operational profiles (e.g. cut-in wind speeds for wind turbines and minimum insolation requirements for solar panels).

We define a compound solar and wind drought as a wind drought and a solar drought occurring on the same day in either the same grid cell or the same REZ, depending on the analysis — Figs. 1, 2, 3 and 4a-c are based on REZ droughts, whereas Fig. 4d-l is based on grid cell droughts. If solar radiation and wind speed were statistically independent processes, we would expect a compound solar and wind drought to occur with an average frequency of 6.25% (0.25^2) over all REZs. Here, we use the term 'compound drought' to describe these events for readability, although according to a typology of compound events, the co-occurrence of two events in one location would be classed as a 'multivariate' event [65].

Much of our analysis focuses on widespread droughts across multiple REZs simultaneously. We adopt two metrics for identifying widespread droughts, both based on REZ-averaged data (i.e. the average of grid cells within each REZ). First, we count the total number of REZs that are in drought each day. We do this separately for solar droughts (for a maximum of 26 per day, which is the number of solar-only plus solar-and-wind REZs), wind droughts (maximum of 29) and compound droughts (maximum of 19). We define a widespread drought as a day on which the number of REZs in drought is in the top 5%. These widespread events are used to generate composite patterns of the atmospheric circulation (Fig. 2). Second, we count the number of REZs affected by drought in each season (JJA, SON, DJF, MAM). The top 10% seasons (seven seasons) are used to obtain composite Southern Hemisphere sea-surface temperature and mean sea-level pressure anomalies (Fig. 3).

Weather and climate diagnostics

We deploy a variety of variables and indices to diagnose the synoptic and large-scale climate associated with renewable energy droughts. To analyse the circulation patterns, we use hourly ERA5 data [64, 66] to compute the daily mean (24 hours from 1400 UTC) 2 m temperature, 500 hPa geopotential height and mean sea-level pressure (MSLP). We also calculate the daytime mean (12 hours from 2000 UTC) fraction of total cloud cover. Anomalies of these variables are obtained by subtracting the full-period day-of-year mean. We use seasonal averages of MSLP computed from monthly ERA5 data [67], and seasonal averages of sea-surface temperature (SST) from the Hadley Centre Global Sea Ice and Sea Surface Temperature data set (HadISST) [68]. Although SST from ERA5 is available, we use HadISST because it provides interpolated observations rather than modelled. Furthermore, HadISST data are assimilated in ERA5 [44]. The monthly MSLP and SST data are converted to anomalies by subtracting the full-period calendar month mean.

The Niño3.4 index [69] is used to represent ENSO, defined as the SST anomaly averaged over 5°N-5°S, 120°-170°W. The Dipole Mode Index (DMI) [70] quantifies the Indian Ocean Dipole (IOD), and is the difference between SST anomalies averaged over western (10°N-10°S, 50°-70°E) and south-eastern (0°-10°S, 90°-110°E) regions in the Indian Ocean. We calculate the Southern Annular Mode (SAM) index from MSLP anomalies as the difference in MSLP anomalies between 40°S and 65°S [71]. For this, the MSLP anomalies are first normalised by dividing them by the monthly standard deviation. In all cases, anomalies are computed by subtracting the full-period calendar month mean.

References

1. DCCEEW. *Australia's emissions projections 2022* tech. rep. (Department of Climate Change, Energy, the Environment and Water, Australian Government, Department of Climate Change, Energy, the Environment and Water, Canberra ACT 2061, 2022). https://www.dcceew.gov.au/sites/default/files/documents/australias-emissions-projections-2022.pdf.

2. Clean Energy Council. *Clean Energy Australia Report 2023* tech. rep. (Clean Energy Council, Clean Energy Council, Level 20, 180 Lonsdale Street, Melbourne VIC 3000, 2023). https://assets.cleanenergycouncil.org.au/documents/Clean-Energy-Australia-Report-2023.pdf.

3. MacGill, I. Electricity market design for facilitating the integration of wind energy: Experience and prospects with the Australian National Electricity Market. *Energy Policy* **38,** 3180–3191. doi:10.1016/j.enpol.2009.07.047 (2010).

4. Bloomfield, H. C., Brayshaw, D. J., Shaffrey, L. C., Coker, P. J. & Thornton, H. E. Quantifying the increasing sensitivity of power systems to climate variability. **11,** 124025. doi:10.1088/1748-9326/11/12/124025 (2016).

5. Staffell, I. & Pfenninger, S. The increasing impact of weather on electricity supply and demand. *Energy* **145,** 65–78. doi:10.1016/j.energy.2017.12.051 (2018).

6. Elliston, B., MacGill, I., Prasad, A. & Kay, M. Spatio-temporal characterisation of extended low direct normal irradiance events over Australia using satellite derived solar radiation data. *Renewable Energy* **74,** 633–639. doi:10.1016/j.renene.2014.08.067 (2015).

7. Evans, J. P., Kay, M., Prasad, A. & Pitman, A. The resilience of Australian wind energy to climate change. *Environmental Research Letters* **13,** 024014. doi:10.1088/1748-9326/aaa632 (2018).

8. Veers, P., Dykes, K., Lantz, E., Barth, S., Bottasso, C. L., Carlson, O., Clifton, A., Green, J., Green, P., Holttinen, H., Laird, D., Lehtomäki, V., Lundquist, J. K., Manwell, J., Marquis, M., Meneveau, C., Moriarty, P., Munduate, X., Muskulus, M., Naughton, J., Pao, L., Paquette, J., Peinke, J., Robertson, A., Sanz Rodrigo, J., Sempreviva, A. M., Smith, J. C., Tuohy, A. & Wiser, R. Grand challenges in the science of wind energy. *Science* **366,** eaau2027. doi:10.1126/science.aau2027 (2019).

9. Engeland, K., Borga, M., Creutin, J.-D., François, B., Ramos, M.-H. & Vidal, J.-P. Space-time variability of climate variables and intermittent renewable electricity production – A review. *Renewable and Sustainable Energy Reviews* **79,** 600–617. doi:10.1016/j.rser.2017.05.046 (2017).

10. Gonzalez-Salazar, M. & Poganietz, W. R. Evaluating the complementarity of solar, wind and hydropower to mitigate the impact of El Niño Southern Oscillation in Latin America. *Renewable Energy* **174,** 453–467. doi:10.1016/j.renene.2021.04.048 (2021).

11. Prasad, A. A., Yang, Y., Kay, M., Menictas, C. & Bremner, S. Synergy of solar photovoltaics-wind-battery systems in Australia. *Renewable and Sustainable Energy Reviews* **152,** 111693. doi:10.1016/j.rser.2021.111693 (2021).

12. Gilmore, N., Koskinen, I., van Gennip, D., Paget, G., Burr, P. A., Obbard, E. G., Daiyan, R., Sproul, A., Kay, M., Lennon, A., Konstantinou, G., Hemer, M., Gui, E. M. & Gurieff, N. Clean energy futures: An Australian based foresight study. *Energy* **260,** 125089. doi:10.1016/j.energy.2022.125089 (2022).

13. AEMO. *Appendix 3. Renewable Energy Zones* tech. rep. (Australian Energy Market Operator (AEMO), 2021). https://aemo.com.au/-/media/files/major-publications/isp/2022/appendix-3-renewable-energy-zones.pdf?la=en.

14. DNV GL. *Multi-Criteria Scoring for Identification of Renewable Energy Zones* tech. rep. (DNV GL - Energy Renewables Advisory, Docklands, VIC, 2018). https://www.aemo.com.au/-/media/Files/Electricity/NEM/Planning_and_Forecasting/ISP/2018/Multi-Criteria-Scoring-for-Identification-of-REZs.pdf (2023).

15. Pezza, A. B., van Rensch, P. & Cai, W. Severe heat waves in Southern Australia: synoptic climatology and large scale connections. *Climate Dynamics* **38,** 209–224. doi:10.1007/s00382-011-1016-2 (2012).

16. Risbey, J. S., McIntosh, P. C. & Pook, M. J. Synoptic components of rainfall variability and trends in southeast Australia. *International Journal of Climatology* **33,** 2459–2472. doi:10.1002/joc.3597 (2013).

17. Quinting, J. F., Catto, J. L. & Reeder, M. J. Synoptic climatology of hybrid cyclones in the Australian region. *Quarterly Journal of the Royal Meteorological Society* **145,** 288–302. doi:10.1002/qj.3431 (2019).

18. Hauser, S., Grams, C. M., Reeder, M. J., McGregor, S., Fink, A. H. & Quinting, J. F. A weather system perspective on winter–spring rainfall variability in southeastern Australia during El Niño. *Quarterly Journal of the Royal Meteorological Society* **146,** 2614–2633. doi:10.1002/qj.3808 (2020).

19. Black, A. S., Risbey, J. S., Chapman, C. C., Monselesan, D. P., II, T. S. M., Pook, M. J., Richardson, D., Sloyan, B. M., Squire, D. T. & Tozer, C. R. Australian Northwest Cloudbands and Their Relationship to Atmospheric Rivers and Precipitation. *Monthly Weather Review* **149,** 1125–1139. doi:10.1175/MWR-D-20-0308.1 (2021).

20. Kahn, E. The reliability of distributed wind generators. *Electric Power Systems Research* **2,** 1–14. doi:10.1016/0378-7796(79)90021-X (1979).

21. Archer, C. L. & Jacobson, M. Z. Supplying Baseload Power and Reducing Transmission Requirements by Interconnecting Wind Farms. *Journal of Applied Meteorology and Climatology* **46,** 1701–1717. doi:10.1175/2007JAMC1538.1 (2007).

22. Huva, R., Dargaville, R. & Rayner, P. Influential Synoptic Weather Types for a Future Renewable Energy Dependent National Electricity Market. *Australian Meteorological and Oceanographic Journal* **65,** 342–355. doi:10.1071/es15024 (2015).

23. Huva, R., Dargaville, R. & Rayner, P. Optimising the deployment of renewable resources for the Australian NEM (National Electricity Market) and the effect of atmospheric length scales. *Energy* **96,** 468–473. doi:10.1016/j.energy.2015.12.082 (2016).

24. Tong, D., Farnham, D. J., Duan, L., Zhang, Q., Lewis, N. S., Caldeira, K. & Davis, S. J. Geophysical constraints on the reliability of solar and wind power worldwide. *Nature Communications* **12,** 6146. doi:10.1038/s41467-021-26355-z (2021).

25. Gunn, A., Dargaville, R., Jakob, C. & McGregor, S. Spatial optimality and temporal variability in Australia's wind resource. *arXiv*. doi:10.31223/X56Q28 (2023).

26. Parker, T. J., Berry, G. J. & Reeder, M. J. The influence of tropical cyclones on heat waves in Southeastern Australia. *Geophysical Research Letters* **40,** 6264–6270. doi:10.1002/2013GL058257 (2013).

27. Millstein, D., Solomon-Culp, J., Wang, M., Ullrich, P. & Collier, C. Wind energy variability and links to regional and synoptic scale weather. *Climate Dynamics* **52,** 4891–4906. doi:10.1007/s00382-018-4421-y (2019).

28. van der Wiel, K., Stoop, L. P., van Zuijlen, B. R. H., Blackport, R., van den Broek, M. A. & Selten, F. M. Meteorological conditions leading to extreme low variable renewable energy production and extreme high energy shortfall. *Renewable and Sustainable Energy Reviews* **111,** 261–275. doi:10.1016/j.rser.2019.04.065 (2019).

29. Bloomfield, H. C., Wainwright, C. M. & Mitchell, N. Characterizing the variability and meteorological drivers of wind power and solar power generation over Africa. *Meteorological Applications* **29,** e2093. doi:10.1002/met.2093 (2022).

30. Davy, R. J. & Troccoli, A. Interannual variability of solar energy generation in Australia. *Solar Energy* **86,** 3554–3560. doi:10.1016/j.solener.2011.12.004 (2012).

31. Prasad, A. A., Taylor, R. A. & Kay, M. Assessment of direct normal irradiance and cloud connections using satellite data over Australia. *Applied Energy* **143,** 301–311. doi:10.1016/j.apenergy.2015.01.050 (2015).

32. Thompson, D. W. J. & Wallace, J. M. Annular Modes in the Extratropical Circulation. Part I: Month-to-Month Variability. *Journal of Climate* **13,** 1000–1016. doi:10.1175/1520-0442(2000)013<1000:AMITEC>2.0.CO;2 (2000).

33. Thompson, D. W. J. & Woodworth, J. D. Barotropic and Baroclinic Annular Variability in the Southern Hemisphere. *Journal of the Atmospheric Sciences* **71,** 1480–1493. doi:10.1175/JAS-D-13-0185.1 (2014).

34. Lim, E.-P., Hendon, H. H., Butler, A. H., Thompson, D. W. J., Lawrence, Z., Scaife, A. A., Shepherd, T. G., Polichtchouk, I., Nakamura, H., Kobayashi, C., Comer, R., Coy, L., Dowdy, A., Garreaud, R. D., Newman, P. A. & Wang, G. The 2019 Southern Hemisphere stratospheric polar vortex weakening and its impacts. *Bulletin of the American Meteorological Society* **102,** E1150–E1171. doi:10.1175/BAMS-D-20-0112.1 (2021).

35. Bianchi, E., Guozden, T. & Kozulj, R. Assessing low frequency variations in solar and wind power and their climatic teleconnections. *Renewable Energy* **190,** 560–571. doi:10.1016/j.renene.2022.03.080 (2022).

36. Kay, G., Dunstone, N. J., Maidens, A., Scaife, A. A., Smith, D. M., Thornton, H. E., Dawkins, L. & Belcher, S. E. Variability in North Sea wind energy and the potential for prolonged winter wind drought. *Atmospheric Science Letters* **24,** e1158. doi:10.1002/asl.1158 (2023).

37. Iizumi, T., Luo, J.-J., Challinor, A. J., Sakurai, G., Yokozawa, M., Sakuma, H., Brown, M. E. & Yamagata, T. Impacts of El Niño Southern Oscillation on the global yields of major crops. *Nature Communications* **5,** 3712. doi:10.1038/ncomms4712 (2014).

38. Anderson, W., Seager, R., Baethgen, W. & Cane, M. Trans-Pacific ENSO teleconnections pose a correlated risk to agriculture. *Agricultural and Forest Meteorology* **262,** 298–309. doi:10.1016/j.agrformet.2018.07.023 (2018).

39. Anderson, W., Seager, R., Baethgen, W., Cane, M. & You, L. Synchronous crop failures and climate-forced production variability. *Science Advances* **5,** eaaw1976. doi:10.1126/sciadv.aaw1976 (2019).

40. Singh, J., Ashfaq, M., Skinner, C. B., Anderson, W. & Singh, D. Amplified risk of spatially compounding droughts during co-occurrences of modes of natural ocean variability. *npj Climate and Atmospheric Science* **4,** 1–14. doi:10.1038/s41612-021-00161-2 (2021).

41. Squire, D. T., Richardson, D., Risbey, J. S., Black, A. S., Kitsios, V., Matear, R. J., Monselesan, D., Moore, T. S. & Tozer, C. R. Likelihood of unprecedented drought and fire weather during Australia's 2019 megafires. *npj Climate and Atmospheric Science* **4,** 1–12. doi:10.1038/s41612-021-00220-8 (2021).

42. Richardson, D., Black, A. S., Irving, D., Matear, R. J., Monselesan, D. P., Risbey, J. S., Squire, D. T. & Tozer, C. R. Global increase in wildfire potential from compound fire weather and drought. *npj Climate and Atmospheric Science* **5,** 23. doi:10.1038/s41612-022-00248-4 (2022).

43. Richardson, D., Kath, J., Byrareddy, V. M., Monselesan, D. P., Risbey, J. S., Squire, D. T. & Tozer, C. R. Synchronous climate hazards pose an increasing challenge to global coffee production. *PLOS Climate* **2,** e0000134. doi:10.1371/journal.pclm.0000134 (2023).

44. Hersbach, H., Bell, B., Berrisford, P., Hirahara, S., Horányi, A., Muñoz-Sabater, J., Nicolas, J., Peubey, C., Radu, R., Schepers, D., Simmons, A., Soci, C., Abdalla, S., Abellan, X., Balsamo, G., Bechtold, P., Biavati, G., Bidlot, J., Bonavita, M., De Chiara, G., Dahlgren, P., Dee, D., Diamantakis, M., Dragani, R., Flemming, J., Forbes, R., Fuentes, M., Geer, A., Haimberger, L., Healy, S., Hogan, R. J., Hólm, E., Janisková, M., Keeley, S., Laloyaux, P., Lopez, P., Lupu, C., Radnoti, G., de Rosnay, P., Rozum, I., Vamborg, F., Villaume, S. & Thépaut, J.-N. The ERA5 global reanalysis. *Quarterly Journal of the Royal Meteorological Society* **146,** 1999–2049. doi:10.1002/qj.3803 (2020).

45. van der Wiel, K., Selten, F. M., Bintanja, R., Blackport, R. & Screen, J. A. Ensemble climate-impact modelling: extreme impacts from moderate meteorological conditions. *Environmental Research Letters* **15,** 034050. doi:10.1088/1748-9326/ab7668 (2020).

46. Pepler, A. S., Dowdy, A. J. & Hope, P. The differing role of weather systems in southern Australian rainfall between 1979–1996 and 1997–2015. *Climate Dynamics* **56,** 2289–2302. doi:10.1007/s00382-020-05588-6 (2021).

47. Rispler, J., Roberts, M. & Bruce, A. A change in the air? The role of offshore wind in Australia's transition to a 100 % renewable grid. *The Electricity Journal* **35,** 107190. doi:10.1016/j.tej.2022.107190 (2022).

48. Risbey, J. S., Pook, M. J., McIntosh, P. C., Wheeler, M. C. & Hendon, H. H. On the Remote Drivers of Rainfall Variability in Australia. *Monthly Weather Review* **137,** 3233–3253. doi:10.1175/2009MWR2861.1 (2009).

49. Holgate, C., Evans, J. P., Taschetto, A. S., Gupta, A. S. & Santoso, A. The Impact of Interacting Climate Modes on East Australian Precipitation Moisture Sources. *Journal of Climate* **35,** 3147–3159. doi:10.1175/JCLI-D-21-0750.1 (2022).

50. L'Heureux, M. L. & Thompson, D. W. J. Observed Relationships between the El Niño–Southern Oscillation and the Extratropical Zonal-Mean Circulation. *Journal of Climate* **19,** 276–287. doi:10.1175/JCLI3617.1 (2006).

51. Gong, T., Feldstein, S. B. & Luo, D. The Impact of ENSO on Wave Breaking and Southern Annular Mode Events. *Journal of the Atmospheric Sciences* **67,** 2854–2870. doi:10.1175/2010JAS3311.1 (2010).

52. van der Ent, R. J., Savenije, H. H. G., Schaefli, B. & Steele-Dunne, S. C. Origin and fate of atmospheric moisture over continents. *Water Resources Research* **46.** doi:10.1029/2010WR009127 (2010).

53. Holgate, C., Evans, J. P., van Dijk, A. I. J. M., Pitman, A. J. & Di Virgilio, G. Australian Precipitation Recycling and Evaporative Source Regions. *Journal of Climate* **33,** 8721–8735. doi:https://doi.org/10.1175/JCLI-D-19-0926.1 (2020).

54. Grams, C. M., Beerli, R., Pfenninger, S., Staffell, I. & Wernli, H. Balancing Europe's wind-power output through spatial deployment informed by weather regimes. *Nature Climate Change* **7,** 557–562. doi:10.1038/nclimate3338 (2017).

55. Bloomfield, H. C., Brayshaw, D. J. & Charlton-Perez, A. J. Characterizing the winter meteorological drivers of the European electricity system using targeted circulation types. *Meteorological Applications* **27,** e1858. doi:10.1002/met.1858 (2020).

56. Toth, Z. & Buizza, R. *Sub-Seasonal to Seasonal Prediction* (Elsevier, 2019). doi:10.1016/B978-0-12-811714-9.00002-4.

57. Ferranti, L., Magnusson, L., Vitart, F. & Richardson, D. S. How far in advance can we predict changes in large-scale flow leading to severe cold conditions over Europe? *Quarterly Journal of the Royal Meteorological Society* **144,** 1788–1802. doi:doi:10.1002/qj.3341 (2018).

58. Lavaysse, C., Vogt, J., Toreti, A., Carrera, M. L. & Pappenberger, F. On the use of weather regimes to forecast meteorological drought over Europe. *Nat. Hazards Earth Syst. Sci.* **18,** 3297–3309. doi:10.5194/nhess-18-3297-2018 (2018).

59. Neal, R., Dankers, R., Saulter, A., Lane, A., Millard, J., Robbins, G. & Price, D. Use of probabilistic medium- to long-range weather-pattern forecasts for identifying periods with an increased likelihood of coastal flooding around the UK. *Meteorological Applications* **25,** 534–547. doi:doi:10.1002/met.1719 (2018).

60. Richardson, D., Neal, R., Dankers, R., Mylne, K., Cowling, R., Clements, H. & Millard, J. Linking weather patterns to regional extreme precipitation for highlighting potential flood events in medium- to long-range forecasts. *Meteorological Applications* **27,** e1931. doi:10.1002/met.1931 (2020).

61. Richardson, D., Fowler, H. J., Kilsby, C. G., Neal, R. & Dankers, R. Improving sub-seasonal forecast skill of meteorological drought: a weather pattern approach. *Nat. Hazards Earth Syst. Sci.* **20,** 107–124. doi:10.5194/nhess-20-107-2020 (2020).

62. Richardson, D., Black, A. S., Monselesan, D. P., Moore II, T. S., Risbey, J. S., Schepen, A., Squire, D. T. & Tozer, C. R. Identifying Periods of Forecast Model Confidence for Improved Subseasonal Prediction of Precipitation. *Journal of Hydrometeorology* **22,** 371–385. doi:10.1175/JHM-D-20-0054.1 (2021).

63. Weisheimer, A. & Palmer, T. N. On the reliability of seasonal climate forecasts. *Journal of The Royal Society Interface* **11,** 20131162. doi:10.1098/rsif.2013.1162 (2014).

64. Hersbach, H., Bell, B., Berrisford, P., Biavati, G., Horányi, A., Muñoz Sabater, J., Nicolas, J., Peubey, C., Radu, R., Rozum, I., Schepers, D., Simmons, A., Soci, C., Dee, D. & Thépaut, J.-N. ERA5 hourly data on single levels from 1940 to present. *Copernicus Climate Change Service (C3S) Climate Data Store (CDS).* doi:10.24381/cds.adbb2d47 (2023).

65. Zscheischler, J., Martius, O., Westra, S., Bevacqua, E., Raymond, C., Horton, R. M., van den Hurk, B., AghaKouchak, A., Jézéquel, A., Mahecha, M. D., Maraun, D., Ramos, A. M., Ridder, N. N., Thiery, W. & Vignotto, E. A typology of compound weather and climate events. *Nature Reviews Earth & Environment* **1,** 333–347. doi:10.1038/s43017-020-0060-z (2020).

66. Hersbach, H., Bell, B., Berrisford, P., Biavati, G., Horányi, A., Muñoz Sabater, J., Nicolas, J., Peubey, C., Radu, R., Rozum, I., Schepers, D., Simmons, A., Soci, C., Dee, D. & Thépaut, J.-N. ERA5 hourly data on pressure levels from 1940 to present. *Copernicus Climate Change Service (C3S) Climate Data Store (CDS).* doi:10.24381/cds.bd0915c6 (2023).

67. Hersbach, H., Bell, B., Berrisford, P., Biavati, G., Horányi, A., Muñoz Sabater, J., Nicolas, J., Peubey, C., Radu, R., Rozum, I., Schepers, D., Simmons, A., Soci, C., Dee, D. & Thépaut, J.-N. ERA5 monthly averaged data on single levels from 1940 to present. *Copernicus Climate Change Service (C3S) Climate Data Store (CDS).* doi:10.24381/cds.f17050d7 (2023).

68. Rayner, N. A., Parker, D. E., Horton, E. B., Folland, C. K., Alexander, L. V., Rowell, D. P., Kent, E. C. & Kaplan, A. Global analyses of sea surface temperature, sea ice, and night marine air temperature since the late nineteenth century. *Journal of Geophysical Research: Atmospheres* **108.** doi:10.1029/2002JD002670 (2003).

69. Trenberth, K. E. The Definition of El Niño in: Bulletin of the American Meteorological Society Volume 78 Issue 12 (1997). *Bulletin of the American Meteorological Society* **78,** 2771–2778. doi:10.1175/1520-0477(1997)078<2771:TDOENO>2.0.CO;2 (1997).

70. Saji, N. H., Goswami, B. N., Vinayachandran, P. N. & Yamagata, T. A dipole mode in the tropical Indian Ocean. *Nature* **401,** 360–363. doi:10.1038/43854 (1999).

71. Gong, D. & Wang, S. Definition of Antarctic Oscillation index. *Geophysical Research Letters* **26,** 459–462. doi:https://doi.org/10.1029/1999GL900003 (1999).

Acknowledgements

The work was undertaken using resources from the National Computational Infrastructure (NCI), which is supported by the Australian government. We acknowledge the Pangeo community for the open-source tools used in the analyses here.

Code availability

The code used for this work is openly available at https://github.com/dougrichardson/AEMO_compound_events.

Data availability

Renewable Energy Zone boundaries can be obtained from https://aemo.com.au/en/energy-systems/major-publications/integrated-system-plan-isp/2022-integrated-system-plan-isp. ECMWF ERA5 reanalysis data for hourly mean surface downward short-wave radiation flux, zonal and meridional wind at 100 m, 2 m temperature, mean sea-level pressure and fraction of total cloud cover are available at https://cds.climate.copernicus.eu/cdsapp#!/dataset/reanalysis-era5-single-levels. ERA5 hourly geopotential height data can be retrieved from https://cds.climate.copernicus.eu/cdsapp#!/dataset/reanalysis-era5-pressure-levels. ERA5 monthly mean sea-level pressure data is from https://cds.climate.copernicus.eu/cdsapp#!/dataset/reanalysis-era5-single-levels-monthly-means. Monthly sea-surface temperature data from the Met Office Hadley Centre Sea Ice and Sea Surface Temperature data set is available from https://www.metoffice.gov.uk/hadobs/hadisst/. Maps in the relevant figures are made with Natural Earth. Free vector and raster map data at naturalearthdata.com. Natural Earth Terms of Use are available at https://www.naturalearthdata.com/about/terms-of-use/.

Author contributions statement

D.R. devised the analysis, wrote the code, produced the figures and wrote the manuscript. D.R., A.P. and N.R. contributed to discussion of results and reviewing of the manuscript.

Competing interests

The authors declare no competing interests.

Supplementary information

Here we provide four figures referred to in the main text. Fig. S1 shows circulation diagnostics (500 hPa geopotential height anomalies and mean sea-level pressure) for the 5% most widespread drought days.

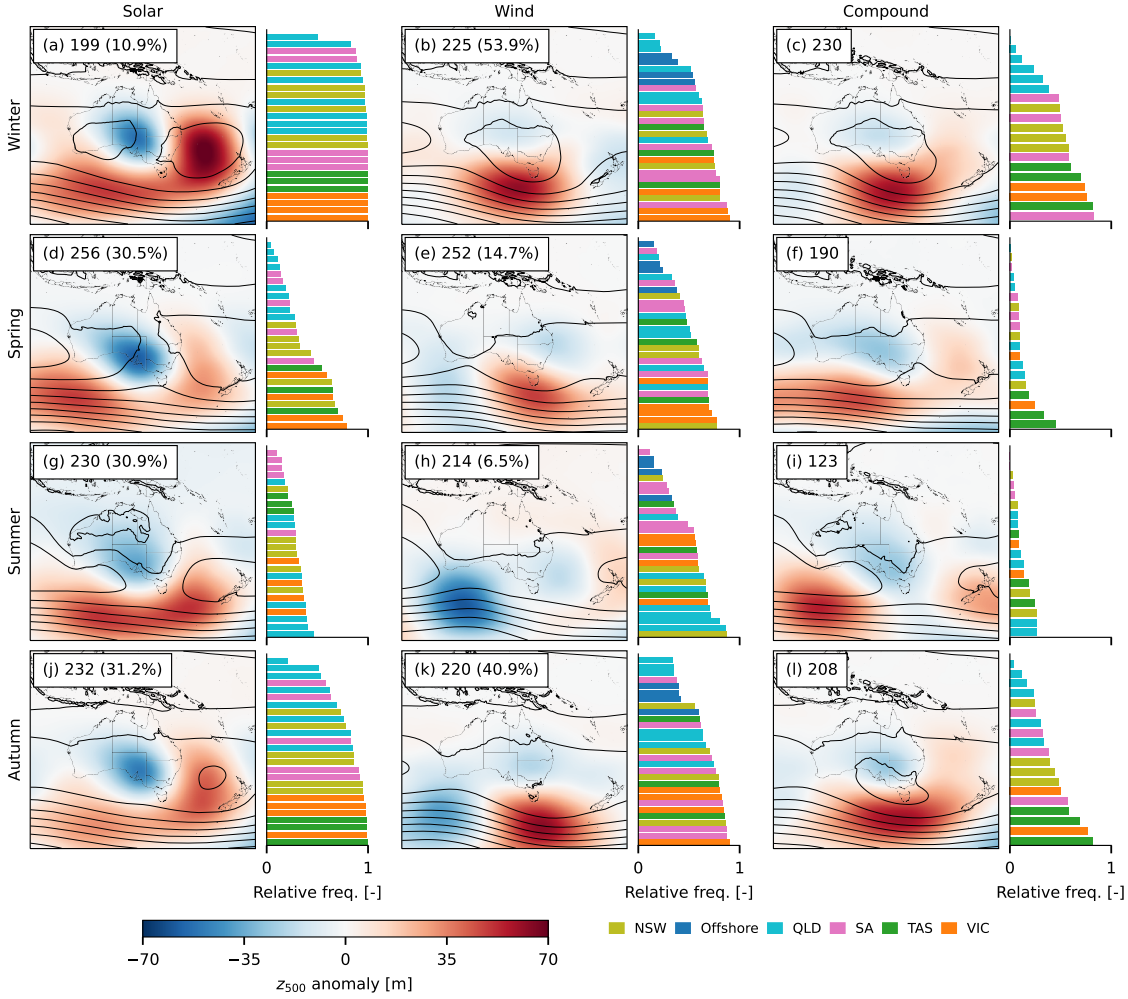

Figure S1. Atmospheric circulation during widespread droughts. Daily composites of the 5% most spatially-extensive drought days by season. The maps show 500 hPa geopotential height anomalies (shading) and full-field mean sea-level pressure (black contours). The sample size of each composite is shown in the top left. For wind and solar droughts, the percentage of days shared with the compound drought composite is shown in parentheses. Bar plots to the right show the relative frequency that each REZ participates in the spatially-extensive droughts that make up each composite, coloured by state.

550 Figures S2, S3 and S4 show the association between seasonal drought frequencies and different phases of each climate mode for spring, summer and autumn, respectively.

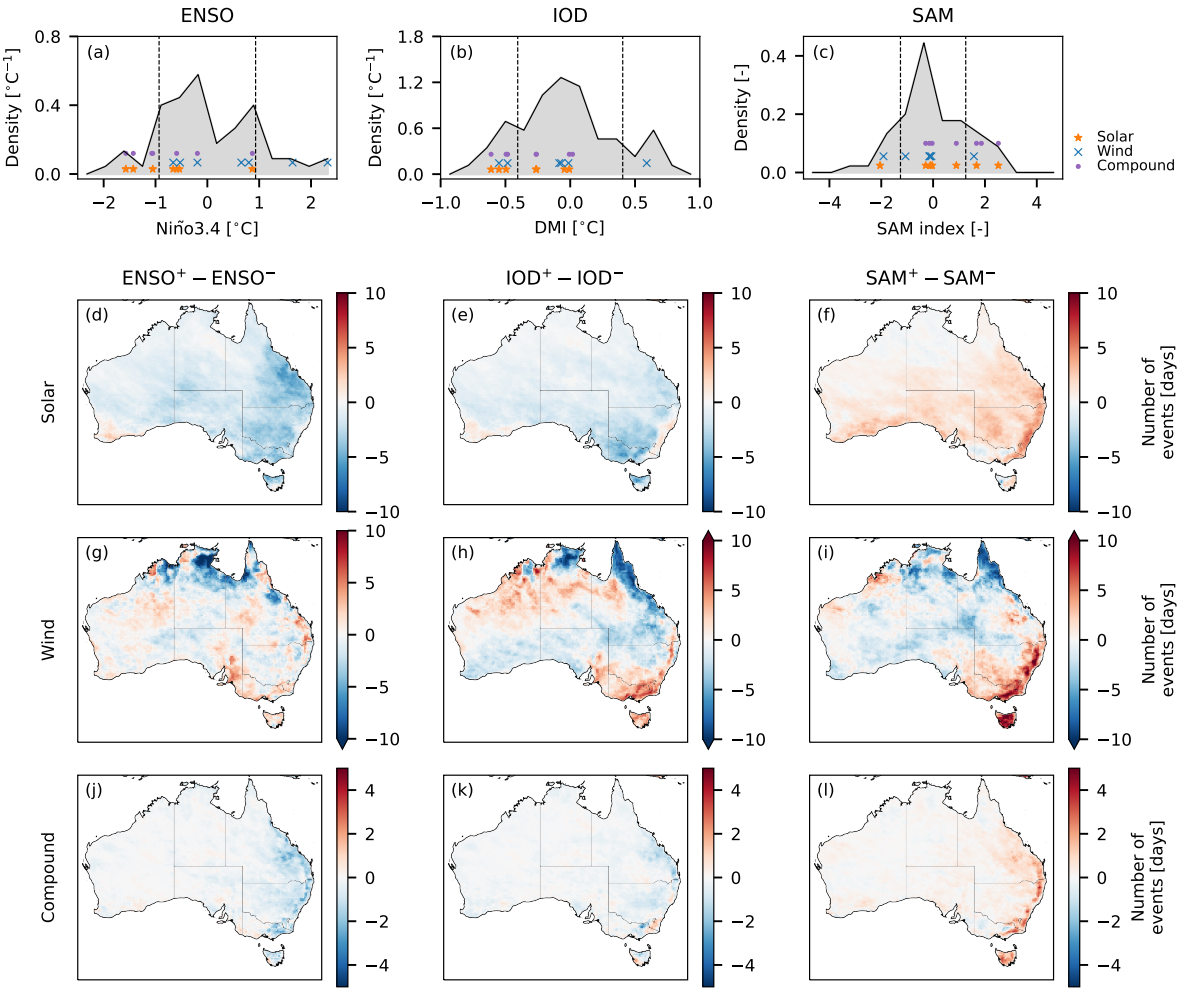

Figure S2. Climate mode influence during spring. a-c Probability density functions of spring-averaged ENSO (measured by Niño3.4), the IOD (DMI) and SAM (SAM index). Dashed lines indicated one standard deviation above or below zero. Markers indicate the mode index value during the seven springs of spatially-extensive droughts shown in Fig. 3. **d-j** Difference in the number of spring drought days between positive and negative phases of each climate mode. A positive phase is when the index value exceeds one standard deviation above the mean, and vice versa for a negative phase. Note the half-magnitude scale for compound droughts compared to in Fig. 3.

551

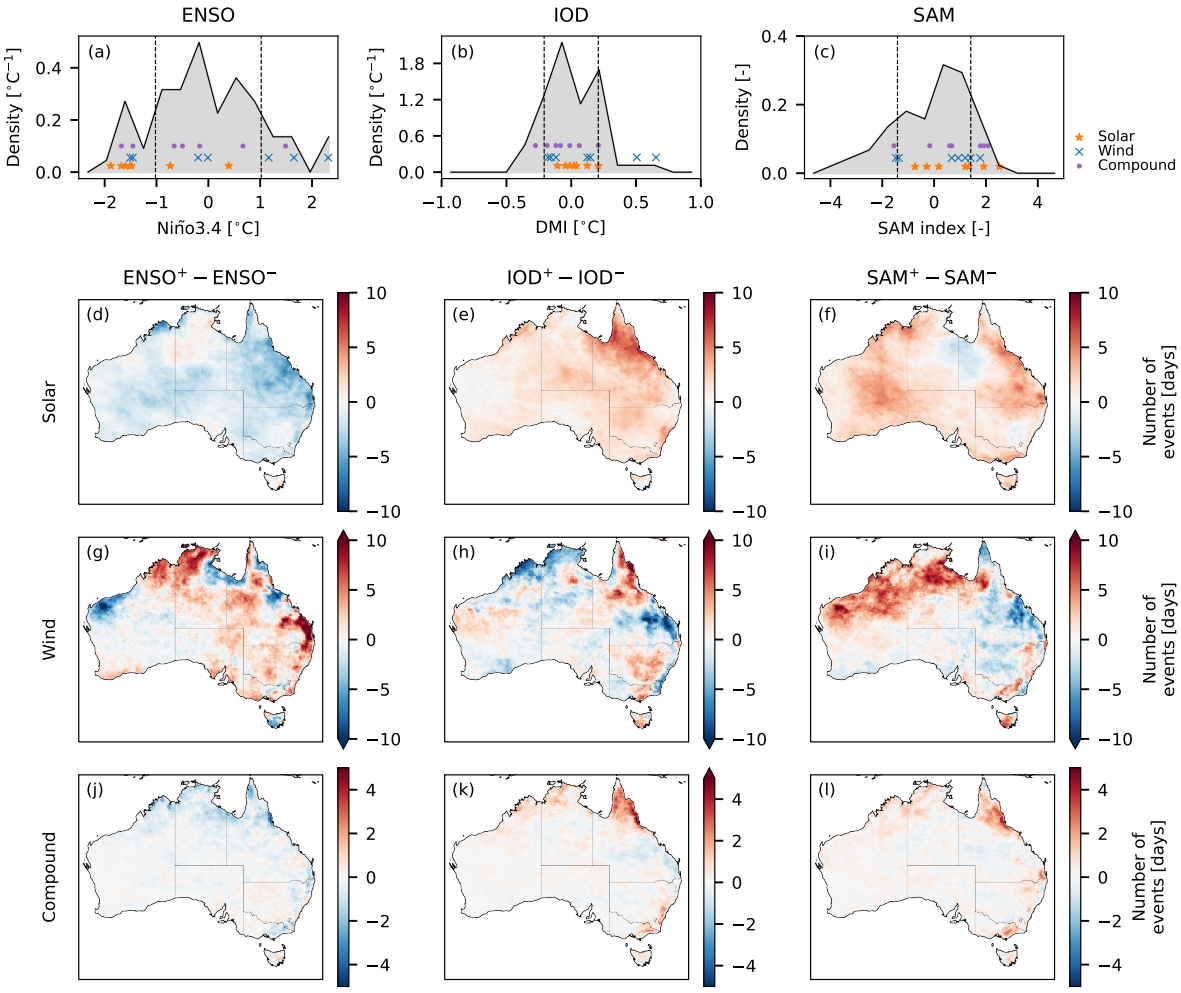

Figure S3. Climate mode influence during summer. As for Fig. S2, but for summer.

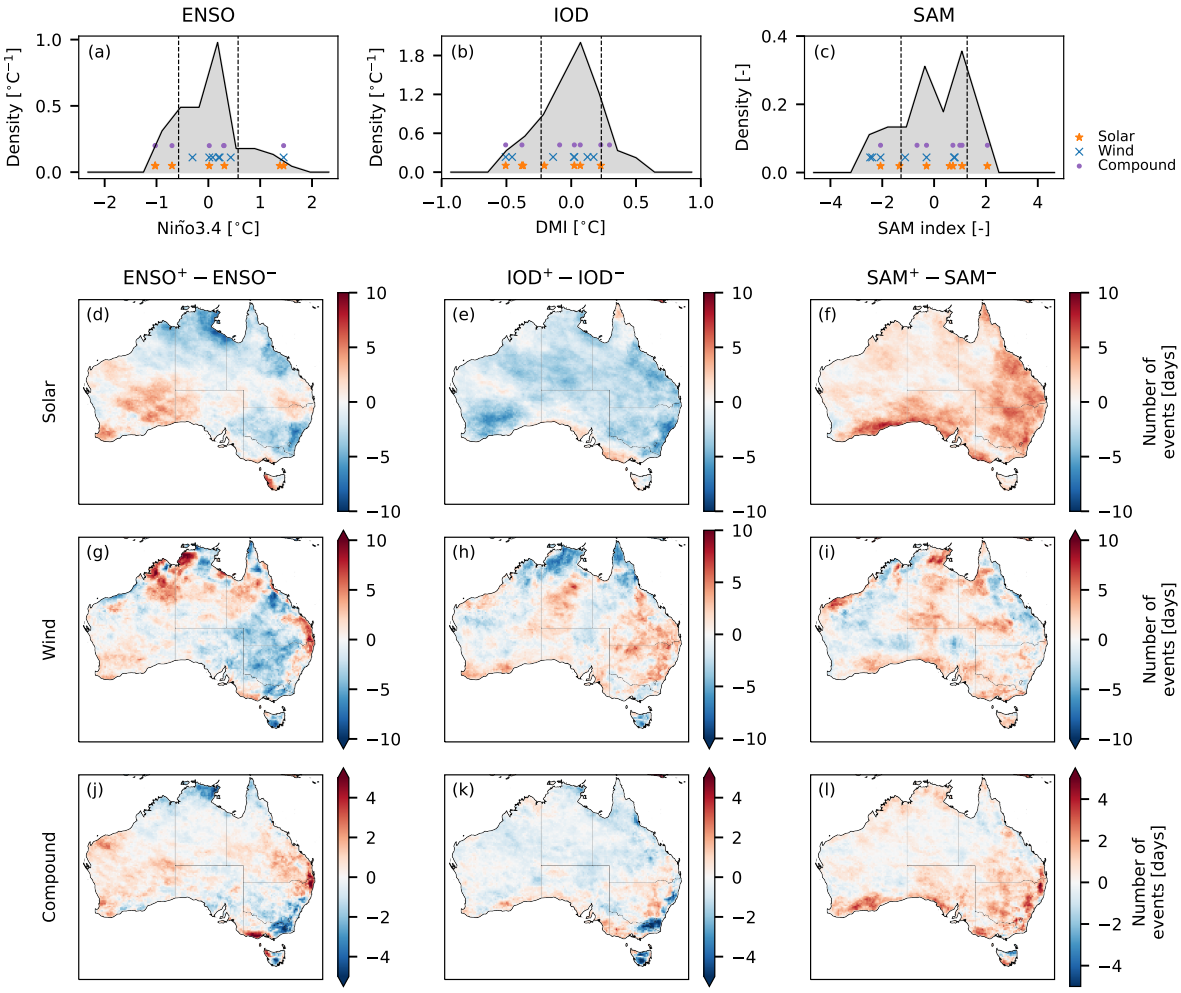

Figure S4. Climate mode influence during autumn. As for Fig. S2, but for autumn.